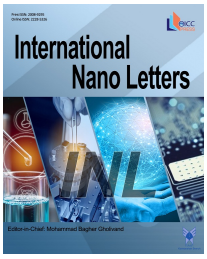

Volume 14, Issue 1, 142404 (1-13)

International Nano Letters (INL)

https://doi.org/10.57647/inl.2024.1401.04

The Effect of Applied Electric Field on Hydrogen Incorporation During the Formation of Au Nanoparticles Fabricated by Laser Ablation

Parisa Ojaroody, Mohammadreza Hantehzadeh*, Elham Darabi

Plasma Physics Research Center, Science and Research Branch, Islamic Azad University, Tehran, Iran.

***Corresponding author:** hantehzadeh@hotmail.com

Original Research

Received:
2 December 2023

Revised:
18 March 2024

Accepted:
20 April 2024

Published online:
30 March 2024

Abstract:

In the present study, gold nanoparticles (NPs) were fabricated by pulsed laser ablation (PLA) method in distilled water environment under different external electric field strengths. The effect of the electric field on the characteristics of produced NPs was traced through X-ray diffraction (XRD), Fourier transforms infrared (FT-IR) and transmission electron microscopy (TEM). Optical properties were studied by UV-visible spectroscopy. The XRD results showed an orthorhombic lattice, alongside the typical cubic structure of Au, which was attributed to the hydrogen incorporation in the crystalline structure of Au nanoparticles. The interaction between hydrogen and gold did not vary linearly with the increased of applied electric field. At an electric field of 20 V/cm, this interaction was almost negligible. Furthermore, the peak observed at around 2000 cm^{-1} in the FT-IR spectrum provided additional evidence for possible Au-H interactions. Based on the TEM images, some non-spherical shapes such as nanorods were successfully synthesized under higher electric field strengths. Moreover, the interaction between hydrogen and gold likely induced a slight blue shift in the UV-Vis spectrum. The formation of Au hydride makes our sample a promising candidate for use as an optical hydrogen sensor; however, further research is needed.

Keywords: Au nanoparticles; Laser ablation; Electric field; Hydrogen incorporation

Cite this article: Ojaroody, P., Hantehzadeh, M., Darabi, E. The Effect of Applied Electric Field on Hydrogen Incorporation During the Formation of Au Nanoparticles Fabricated by Laser Ablation. *Int. Nano Lett.* **14**(1), 142404 (2024).

1. Introduction

Nanoparticles made from noble metals are promising candidates for various applied research fields, including catalytic activity, optics, medicine, sensors, and diagnostics [1–3]. Among the various noble metals, gold NPs, as a 5d metal, have attracted significant attention and have emerged as a leading candidate for a wide range of applications, including drug delivery vectors and biological imaging [3], optical and electrochemical sensors and solar cells [4]. Moreover, gold NPs are well-known for their wide-ranging bio sensing applications, owing to their unique physicochemical properties, ease of synthesis, and exceptional optical characteristics, which vary with size, shape and aspect ratio. These distinctive features of gold NPs facilitate the detection and sensing of biological molecules and chemical compounds, making them valuable across various industrial sectors [5]. For example, numerous researchers are concentrating on food safety detection due to the potential hazards that substances in food can pose to human health. Consequently, ensuring food safety has emerged as a significant global challenge. In this context, gold NPs, which are available in various shapes, can serve as effective probes. These minuscule particles exhibit unique properties that can be harnessed to develop biosensors for detecting a range of contaminants [6]. Moreover, gold NPs in the form of gold hydride, which is a rare transition metal hybrid with an Au-H structure, are believed to play a crucial role in gold-catalyzed reactions, including hydroboration and hydrogenation [7]. The formation of Au-H presents a promising candidate for application as an optical hydrogen sensor [8, 9]. The diverse applications and requirements for particle variety-including size, geometric shape, and composition-have driven the development of various synthesis methods. Each of these methods, which include chemical reduction, microbial synthesis, and the sol-gel process, has its own advantages and disadvantages [10]. However, the limitations of these methods

include difficulties in controlling NPs morphology, ensuring reproducibility, and achieving sustainability [4]. Recently, PLAL has emerged as a versatile and environmentally friendly method for fabricating a variety of organic and inorganic NPs. This technique is noteworthy for its simplicity, distinctive surface chemistry, ability to produce contaminant-free samples, and capacity for controlling NPs size [11–14]. The sequence of laser ablation processes involves the generation of plasma through laser ablation, the energy transfers from the plasma to the liquid, and the subsequent formation and release of bubbles into the solution [15]. In comparison to other types of lasers, such as picosecond and femtosecond lasers, nanosecond lasers are more commonly utilized in PALA. Nanosecond laser pulses ablate material primarily through two mechanisms: (1) explosive ejection of molten material, in droplet form ranging from nanometers to micrometers, induced by thermal stress; and (2) thermal vaporization of the target material into atomic or ionic species from the surface [16]. The colloidal nanoparticles prepared using this method are evaluated based on their versatility, purity, electrical affinity, and the availability of precursors [17]. Compared to other techniques, this method is prioritized for its versatile approaches and rapid production of NPs without toxic substances or contamination. As a result, it is highly beneficial for biomedical applications [18–20]. It is observed that NPs can be generated in a confined plasma through the processes of nucleation and coalescence via laser ablation [21–23]. This renders the technique highly versatile, as it can be used to fabricate semiconductors, metals, oxides, alloys, and even core-shell structures [10]. It is possible to achieve higher production rates while enhancing the control over morphology and size, by optimizing the setup design and laser parameters such as, wavelength and laser power [24–26]. Furthermore, the use of electrical fields assisted by laser ablation in liquids (EFLAL) can enhance the control over the morphology, size, and chemical composition of nanoparticles. This technique represents a significant option for the fabrication of NPs with specialized morphologies and crystalline properties [27, 28]. Indeed, numerous charged particles-such as electrons, ions, and ionized species-present in the surrounding liquid can be influenced by an electric field. Consequently, the dynamic behavior of charged particles and charge distribution within the plasma plume is significantly affected by the application of an electric field. As a result, the processes involved in generating nanoparticles with and without the application of an external electric field during the laser ablation can be fundamentally different [29]. Application of an external electric field can effectively inhibit the agglomeration of nanoparticles. The laser-generated plasma consists of free electrons, ions, vapors, and nanodroplets. While, the distribution of electric charges is altered, leading to a decrease in the rate of electron-ion recombination [27]. Furthermore, the enhancement of the electric field within the plume may improve the rate of electron confinement within the nanodroplets. As a result, it is plausible that the application of an external electric field could enhance the charge of these nanodroplets. Based on the principles of electrostatic interaction and Rayleigh instability, an increase in the charge of the nanodroplets typically results in a reduction in their size, leading to deformation. This mechanism arises when the electric field induces charge separation, causing the droplet to behave as a dipole, which can also result in an elongated shape [27–30]. To date, numerous studies have been conducted on controlling NPs through external fields facilitated by laser ablation. A comprehensive review of the effects of EFLAL, including temperature, magnetic, and electric fields, was presented by J. Xiao et al. [31]. They demonstrated that external electric field can effectively regulate the morphology of nanoparticles prepared by laser ablation method. The applied electric field, the wavelength of the laser, and the types of liquids are the most important factors that can influence the structural, physical, and optical properties of the samples examined by Moniri et al. [30]. Mozaffari et al. conducted a study to investigate the enhancement of the ablation rate from an aluminum target irradiated by a pulsed laser in the presence of an electric field within an ethanol solution [32]. Two distinct experimental configurations, namely parallel and perpendicular arrangements, were employed in the study. Aggregation and orientation have been demonstrated to play a crucial role in the formation of CuO nanospindles in the presence of external electric field. Specifically, this mechanism involves the growth of larger particles from smaller ones through a process known as oriented attachment, as examined by Lin et al. [33]. Razaghianpour et al. reported that the application of an external electric field during pulsed laser ablation of Cu in ethanol decreased the nanoparticle size and caused a blue shift in the surface plasmon resonance. Also, the results indicated that the electric field impact plasma dynamics and surface charge accumulation, which in turn governed the size and morphology of the nanoparticles [34]. One of the significant benefits of utilizing an electric field is the enhancement of NPs production rates. The ablation rate presents a considerable challenge when using pulsed laser ablation PLA. Various methods have been developed to address this issue, including rotating targets [35], the double pulse technique [36], and wire targets in a liquid jet [37], all of which have been shown to increase laser absorption and improve nanoparticle production efficiency. In addition to these methods, the application of an external electric field can effectively enhance laser absorption, increase the metal removal rate, and improve the overall production of NPs [38]. This study could build upon previous research investigating the production of gold NPs via the laser ablation in water under an applied electric field, two different electric field being tested [27]. The current experiment will utilize a broader range of electric field. We will demonstrate that applying an external electric field during laser ablation will enable precise control over nanoparticle size and physical characteristics. This controlling provides the basis for establishing a reliable database that links synthesis parameters to nanoparticle properties, paving the way for sensor fabrication and other industrial applications. Such a database can further enable automated optimization of fabrication through algorithms, artificial intelligence and feedback-based control systems ultimately supporting a fully reproducible and scalable nanoparticle production line

[39]. Also, the plasma conditions generated by the laser are modified by the applied electric field, suggesting that non-spherical NPs may form under certain experimental conditions. The fabrication of non-spherical NPs presents a significant challenge, yet it holds substantial industrial applications [29–40]. Additionally, in our experiment, the laser pulse generated a transient plasma with extremely high temperature and localized pressure. This energetic plasma environment may facilitate interactions between hydrogen and gold - similar to those observed metal hydrides by the high- pressure hydrogen technique described by Degtyareva [41].

2. Materials and methods

Methodology

Gold NPs were synthesized using laser ablation of a gold plate in deionized water. In this experiment, we exclusively utilized deionized water and a gold metal plate with the purity of 99.99%. No chemical additives were intentionally introduced into the solution. The ablation source employed in this study was a Q-switched Nd:YAG laser (Q-PLUS model from Spectrum A.T.N. Ltd). The first harmonic wavelength was set at 1064 nm, with a specific repetition rate of 10 Hz, a pulse width of 7 ns, and a total of 3000 laser shots applied to each sample. The use of this wavelength is preferred over its second harmonic at 532 nm due to greater absorption by water molecules, which increases the likelihood of ionization and interaction with gold plasma [42, 43]. Furthermore, previous studies have demonstrated that water provides the optimal environment for achieving a uniform size distribution of nanoparticles during laser ablation [27]. Before the experiment, the gold rectangular target (1 mm thickness, 99.99% purity) was polished using a 1500-grade emery paper to achieve clean metal surfaces. Following this, the target was thoroughly cleansed with distilled water, acetone, and absolute ethanol using an ultrasonic device for 30 minutes to remove any contaminants. The polished target was then securely fixed to the bottom of a Pyrex vessel which is rectangular with dimensions of $8 \times 5.5 \times 4.5$ cm^3. A total of 30 mL of distilled water was added to the vessel, creating a liquid environment with a depth of approximately 6 mm above the target. Figure 1 presents the schematic illustration of the experimental setup. As shown, the laser beam was delivered perpendicularly to the target surface with a flounce of 1.5 J/cm^2, using a plane mirror and an objective lens with focal length of 10 cm. The laser spot size on the target surface was 40 μm for the wavelength of 1064 nm. The laser beam was concentrated by an especial objective lens to a point around 6 mm in diameter. Two gold electrodes (2×2.6 cm^2), also with 99.99% purity, were positioned 20 mm apart from each other, parallel to the sides of the vessel and within the liquid. An adjustable potential was applied to two electrodes positioned on either side of the target. The applied potential were 0, 10, 20, 30, 40, and 50 V, corresponding to the electric field magnitudes of 0, 5, 10, 15, 20, and 25 V/cm, respectively. During the experiment, both the gold target and distilled water were maintained at room temperature. The ablation process lasted approximately 15 minutes for all samples. The production of gold NPs was attributed to the interaction between a laser beam and an electric field. In this experiment, the colloidal solution exhibited various colors before and after irradiation, ranging from colorless to yellowish-brown, depending on different values of the electric field, as illustrated in Fig. 2.

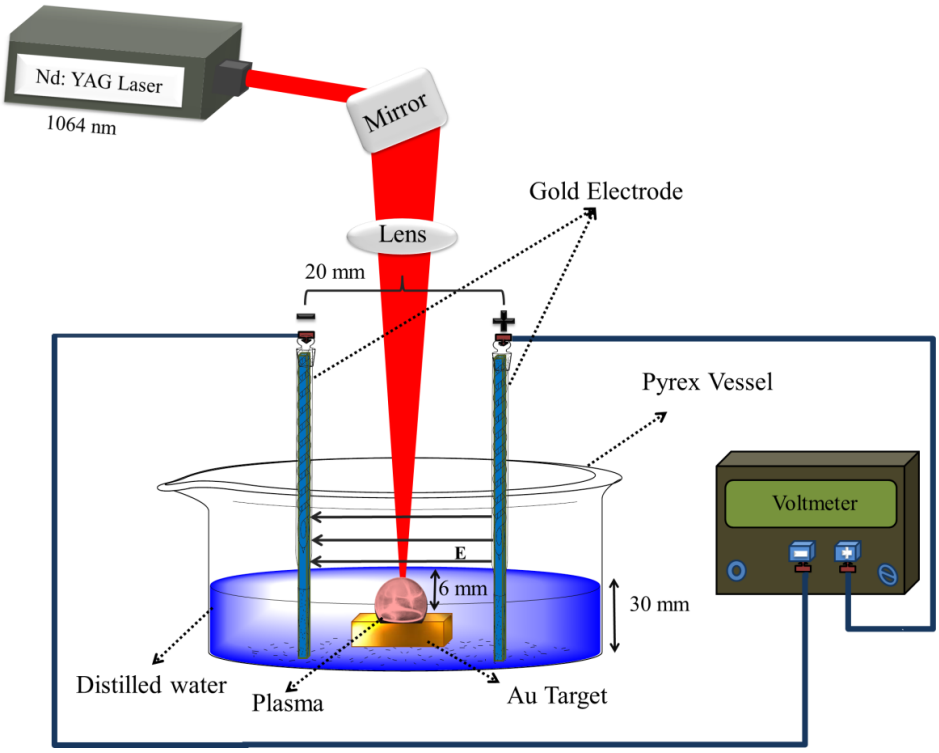

Figure 1. Schematic illustration of experimental setup.

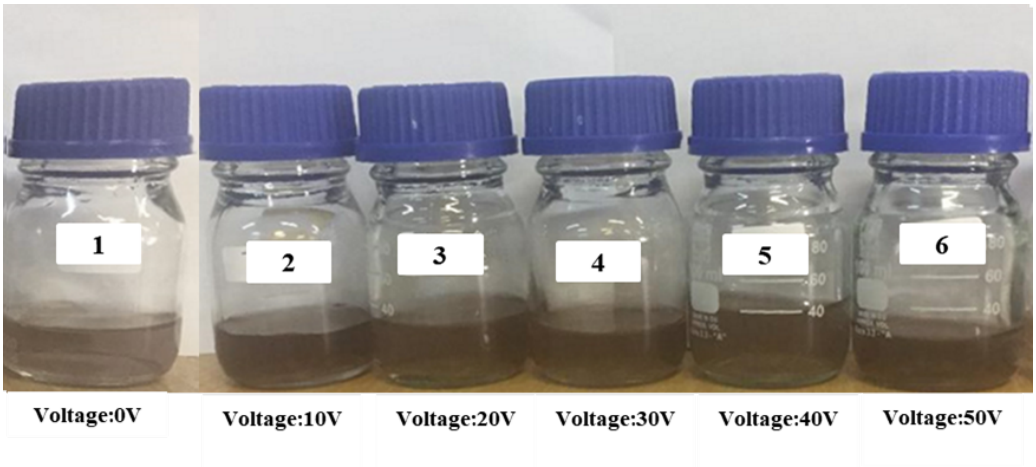

Figure 2. Photos of the synthesized colloidal gold NPs by laser ablation at different voltages corresponding to electric field of 0, 5, 10, 15, 20 and 25 V/cm.

Characteristics

Extensive diagnostics were conducted to examine the characteristics of the products. The crystalline structure of the samples was investigated using an XPERT PRO (Philips PW 1730) XRD with Cu Kα radiation ($\lambda = 1.5406$ Å). To obtain XRD data, several drops of the suspensions were dried on a silicon substrate to create XRD patterns of gold NPs. For TEM, one drop of the concentrated suspension was applied to a carbon-coated copper grid and dried, utilizing a Philips CM120 operating at 100 kV, manufactured in the Netherlands. The chemical bonds within the samples were analyzed using FTIR spectroscopy (Spectrum Two from PerkinElmer, USA). The optical absorption spectra of the samples were analyzed at room temperature in a 10 mm quartz cell using a UV-VIS spectrophotometer (Biomate 5 model) from Thermo Fisher Scientific, USA, operating within the wavelength range of $190 - 1100$ nm. Zeta potential analyses was conducted using a ZetaSizer device from Malvern Instruments, UK.

3. Results and discussion

The effect of external electric fields on the crystalline structure of synthesized gold NPs is depicted in figure 3. X-ray diffraction analysis revealed significant variations in the crystallographic structure and the positions of the diffraction peaks of the generated gold NPs, contingent upon the application of an electric field. Notably, when the maximum electric field was applied, diffraction peaks corresponding to the (200) and (111) crystal planes of face-centered cubic gold were observed. On the other hand, the (200) crystal plane was detected in the absence of an electric field (JCPDS Card File No. 00-001-1174) [44]. Furthermore, in other samples, the structure of the gold NPs exhibited a rightward shift. The peak observed at approximately $2\theta = 30°$ corresponds to the silicon substrate. Additionally, the ablation method facilitated the growth of the Au_2O_3 oxide phases. The pattern was observed at 0 V/cm and at angles of 61.48°, which were consistent with JCPDS Card File No. 00-043-1039. This peak is indicative of the presence of gold NPs associated with the formation of a crystalline Au oxide structure. Across the other applied electric fields, the formation of Au_2O_3 appears probable, consistent with the trends depicted in the corresponding figure 3. It can be claimed during ablation process the bond of gold atoms breaks by energy of laser pulses and these atoms recombine again in the cooling stage. In this time, some Au atoms combine with oxygen atoms in the solution to form gold oxides molecules [45]. In accordance with Bragg's Law, the lattice spacing (dhkl) corresponding to the (330) reflection of the orthorhombic structure of gold has been determined for the nanoparticles [46]. The average crystalline size of nanoparticles was determined using the full width at half maximum (FWHM) of the (330) diffraction peak based on the Scherer equation [47]. The calculated crystalline size of Au NPs was evaluated to be 7.7, 21.4, 21.1 ,18.4, 20.1 and 16.9 nm, corresponds to the sample prepared under external electric field of 0, 5, 10, 15, 20, 25 V/cm, respectively. Surprisingly, in addition to the well-known cubic structure of Au, an orthorhombic lattice corresponds to AuH_x compound was observed, which aligns most closely with the $AuH_{0.35}$ structure (JCPDS No. 00-036-1209). The cell volume for pure gold in its cubic structure is 67.41 nm^3, while the volume of $AuH_{0.35}$ is increased due to the incorporation of additional hydrogen atoms into the Au lattice structure, resulting in the formation of a hydride compound with a cell volume of 512.98 nm^3. Generally, the increase in volume observed in metal hydride groups can be attributed to the interaction between the hydrogen electron and the valence bond of the host metal, which is mainly composed of d and s orbits [41]. During the laser ablation process, hydrogen species can interact directly with the surface of gold NPs. The surface electronic states of gold, located close to the Fermi level, enable charge redistribution between hydrogen and the metal surface. This interaction leads to the formation of weekly bonded surface complexes, indicating a partial incorporation or adsorption of hydrogen atoms on the nanoparticle surface. As the particle size decrease, the surface –to- volume ratio increase, providing more active sites for hydrogen adsorption. The observed variability in hydrogen adsorption on gold NPs produced by laser ablation is strongly influenced by the applied electric field. At certain electric fields, electron transitions from the fermi

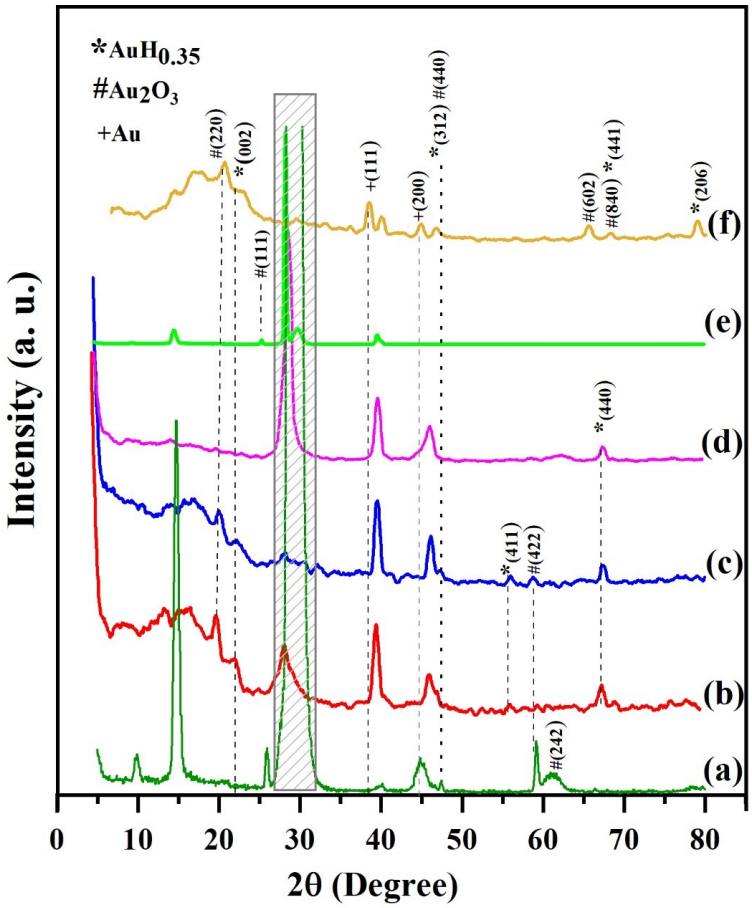

Figure 3. XRD spectra of the synthesized colloidal gold NPs by the laser ablation at electric fields of: (a) 0 V/cm, (b) 5 V/cm, (c) 10 V/cm, (d) 15 V/cm, (e) 20 V/cm, (f) 25 V/cm.

level of the gold NPs to the antibonding orbitals of hydrogen are energetically favorable, promoting adsorption. While, at other electric fields this process is suppressed [48, 49]. In our experiment, the observed formation of a minor amount of $AuH_{0.35}$, as evidenced by X-ray diffraction data, indicates that water undergoes partial decomposition during the process – a factor that contributes significantly to the emergence of this hydride compound. In this ablation procedure, the generation of Au plasma results from the high pressure and temperature induced by the laser pulse. Concurrently, reactive OH/H species produced from the water decomposition surround the plasma and interact with Au^+, leading to the formation of $AuH_{0.35}$ alongside the primary gold NPs [31]. The experimental observations indicated that the formation of gold –hydrogen nanostructures under the applied electric fields was week. The low intensity of the corresponding peaks suggested that the interaction between hydrogen species and the gold surface was not sufficiently strong to produce stable chemical bonding. In addition, although a weak Au-H hybrid peak was observed under most applied electric field conditions (as shown in Fig. 3), it seems that no interactions or very weak interactions occur between hydrogen and gold in the electric field of 20 V/cm. In fact, the formation of hydrides generally exhibits a non-monotonic behavior with respect to the applied electric fields [48, 49]. Under the electric field of 20 V/cm, it is assumed that the plasma conditions- including plasma density, hydrogen availability and surface interaction time – are not favorable for stabilizing Au-H bonds, and as a result, hydride formation is suppressed. To date, numerous transition metal hydrides have been synthesized using the high-pressure hydrogen technique [41]. In this report, we observed interactions between gold and hydrogen during laser ablation synthesis in the presence of an electric field. Gold hydrides, as a class of transition metal species, are utilized in gold-catalyzed reactions. Therefore, the production of $AuH_{0.35}$ represents a significant advancement in this field [7].

Figure 4 presented the TEM images and figure 5 illustrated the size histograms of gold NPs produced under varying electric fields. The approximate size of the gold NPs was determined by Digimizer software, yielding average sizes of 10 – 20, 4.5 – 6.5, 5 – 12.5, 6 – 10, 20 – 24, 15 – 30 nm for electric fields of 0, 5, 10, 15, 20, and 25 V/cm, respectively. Also, the synthesized gold nanorod had an average length of 103 nm and a diameter of 19 nm , in the electric field of 15 V/cm. The images indicate two distinct types of size distribution, initially, the formation of larger particles is anticipated as the laser beam ablates the surface. However, with continuous laser ablation, the occurrence of secondary ablation becomes inevitable. Primary particles exposed to the laser may be re-irradiated, leading to their fragmentation into smaller nanoparticles [45]. Consequently, we observed two distinct size distributions: one

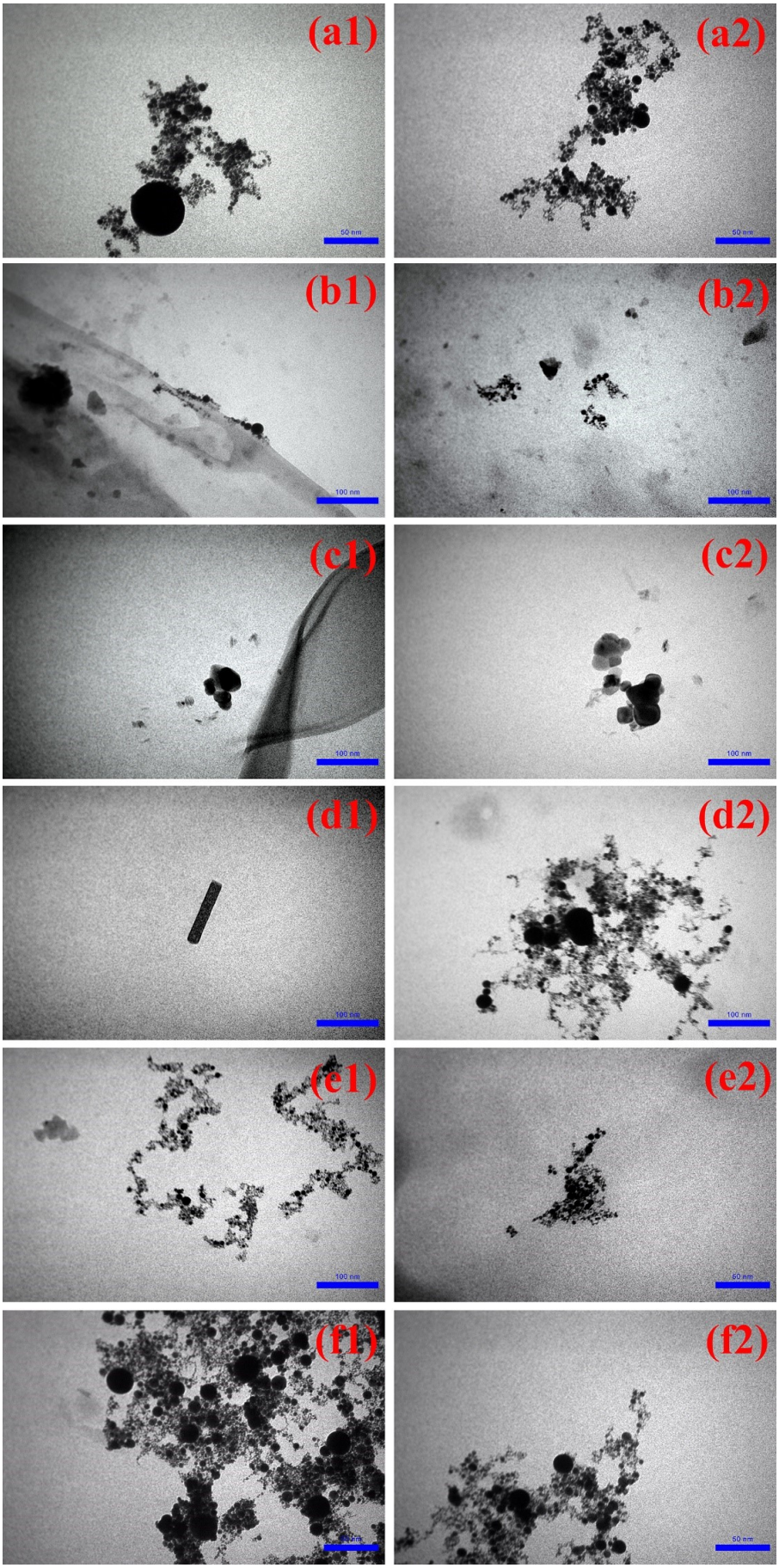

Figure 4. TEM images of the synthesized colloidal gold NPs at electric fields of: (a) 0 V/cm, (b) 5 V/cm, (c) 10 V/cm, (d) 15 V/cm, (e) 20 V/cm, (f) 25 V/cm.

comprising small nanoparticles with a narrow size distribution and another with larger nanoparticles, a phenomenon previously reported for nanoparticles fabricated via pulsed laser ablation in liquid [1]. The figure 4 indicated that at lower electric field, insufficient field strength limits particle separation and enhances aggregation, resulting in large, less dispersed gold nanoparticles (electric field of 0, 5, 10 V/cm). Under stronger electric field conditions, more energetic plasma species are generated, leading to enhanced charge separation and increased coulomb repulsion. These effects suppress particle coalescence, resulting in well, dispersed gold nanoparticles (electric field of 15, 20 V/cm) [27, 50]. Moreover, as the electric field increased, some non-spherical shapes emerged. Notably, we observed rod-like nanoparticles when the applied electric field was set to 15 V/cm. Although nanoparticles naturally adopt a spherical morphology, which is thermodynamically more stable, the application of an external electric field introduces additional energy in to the system, enforcing preferential growth along specific crystallographic planes. leading to the formation of gold NPs with distinct morphologies. In other words, stronger electric fields alter the crystal growth by promoting anisotropic growth along preferred crystallographic orientations. Such field- induced anisotropy facilitates particle elongation along specific directions and suppresses growth in others, leading to the formation of non- spherical morphologies [51, 52]. Besides, by increasing the electric field strength, the nanodroplet generated by laser ablation acquire additional charges. The external field induces charge separation within each droplet, rendering them elongated and dipolar. These electrostatic interactions in the colloidal medium not only influence particle stability and morphology but also affect their size. As a result, the droplet adopts non- spherical shapes, which mitigates the onset of Rayleigh instability and reduces their propensity for fragmentation [28, 38]. Also, analysis of TEM images revealed that, upon applying the maximum voltage, all irregular shapes diminished, and spherical gold NPs became predominant. This phenomenon is likely related to Rayleigh instability, which can be explained as follows: As the strength of the applied electric field increases, the charge of the Nano droplets inevitably increases. Consequently, the charge of these Nano droplets in the liquid state affects their size distribution due to Rayleigh instability [38, 53]. We hypothesize that at 25 V/cm, the charge exceeded a critical threshold, resulting in droplet instability and ultimately leading to the formation of smaller fragments.

The UV-VIS absorption spectra of the synthesized gold NPs under varying electric field strengths are presented in figure 6. The peaks corresponding to localized surface Plasmon resonance (LSPR) for all samples at electric field values of 0, 5, 10, 15, 20, and 25 V/cm were observed in the visible region, indicating the metallic nature of the gold NPs. Upon increasing the particle size of gold NPs, the surface Plasmon resonance band shifts toward longer wavelengths (red shift). Conversely, reducing the particle size results in a blue shift toward shorter wavelengths [44]. The results indicate that, while the positions of all peaks remained relatively stable, we observed slight blue and red shifts at varying electric field. Additionally, small peaks around 1000 nm can be attributed to a few larger particles observed in the TEM images, with their absorbance values being lower than that of the main peak. We investigated the effect of hydrogen incorporation in to the gold lattice using UV-Vis spectroscopy. At each electric field, where an XRD peak indicative of AuH appeared, a corresponding blue shift was detected in the UV-Vis absorption spectra. In previous research conducted by Sil and colleagues (2019), a blue shift in the UV-Vis spectra was observed. This phenomenon indicates that the incorporation of hydrogen into the lattice modifies optical properties, leading to a shift of absorption features or scattered light toward shorter wavelengths [54]. In our experiment, based on the XRD analysis, we assumed that the interaction between hydrogen atoms and gold NPs is more probable under an electric field strength of 10 V/cm, which induce a slight blue shift in the UV-

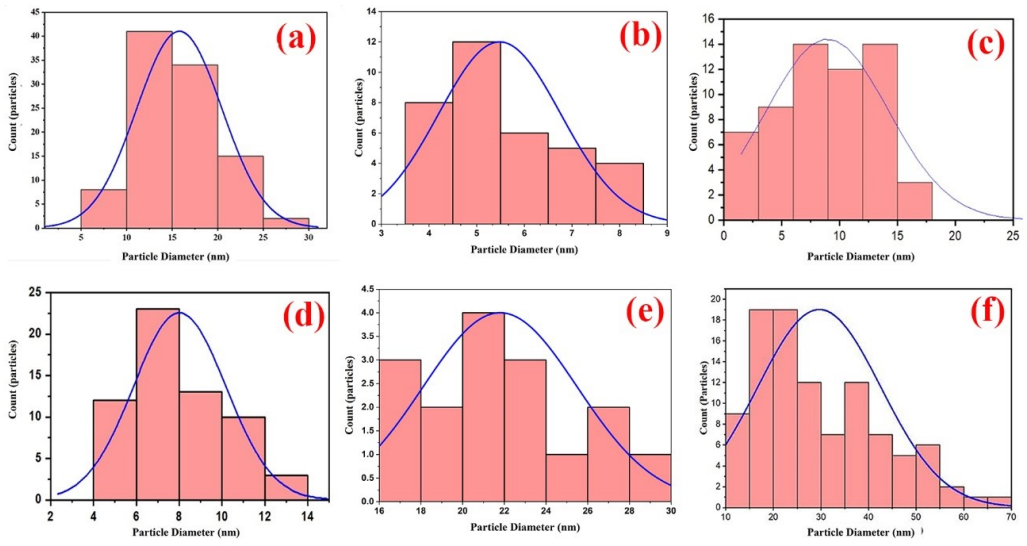

Figure 5. The size distribution of the synthesized colloidal gold NPs at electric fields of: (a) 0 V/cm, (b) 5 V/cm, (c) 10 V/cm, (d) 15 V/cm, (e) 20 V/cm, (f) 25 V/cm.

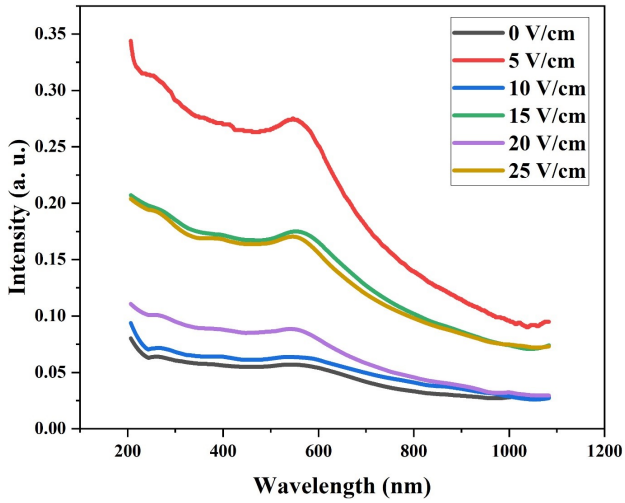

Figure 6. UV-Vis absorption spectra of the synthesized colloidal Au NPs at electric field of 0, 5, 10, 15, 20 and 25 V/cm.

vis spectra. In fact, at lower electric fields strengths, the field is not sufficient to completely separate hydrogen from gold surface, making the interaction between them more probable. In addition, under an applied electric field of 15 V/cm, a slight red shift observed, which can be attributed to the presence of non-crystalline nanoparticles detected in TEM. The non –spherical nature of these nanoparticles appears to cause the UV-Vis peak to shift toward longer wavelengths [55]. Moreover, a red shift was observed at an electric field of 25 V/cm compared to 0 V/cm which could be attributed to the electric-field –induced migration of gold NPs toward the electrode. The enhance collisions and subsequent aggregation of the migrating nanoparticles increase their effective size, leading to a red –shift in the surface plasmon resonance peak [27]. This interpretation is supported by the TEM analysis, which shows that average particle size increase from approximately 20 nm at an electric field of 0 V/cm to about 30 nm at an electric field of 25 V/cm, confirming that the red shift originates from the field-induced aggregation and growth of nanoparticles. Table 1 illustrated Surface Plasmon resonance (SPR) as well as the main absorption peak for gold NPs at different magnitude of applied external electric field.

Figure 7 presented the FTIR spectra used to identify any adsorbed species across different electric fields, reported within the spectral range of 4000 to 400 cm^{-1}. Overall, the samples fabricated under various electric fields (0, 5, 10, 15, 20, and 25 V/cm) exhibited similar absorption bands without any noticeable shifts. However, the profiles of the bonds varied with the applied electric fields. Notably, the profiles at 10 and 15 V/cm displayed distinct characteristics compared to the others which was explained later in this section. The prominent and robust absorption band observed at around 3600 and 3200 cm^{-1} is associated with the vibrational modes of the hydroxyl group (OH), as well as the O-H stretching bonds in water molecules [56]. It is hypothesized that interactions occur between the O-H groups and metal nanoparticles [57]. Consequently, this bond can alternatively be represented as Au-OH. Additionally, the spectral peaks observed in the vicinity of 3000 cm^{-1} correspond to the C-H stretching vibrations [58]. The bond observed at approximately 1650 cm^{-1} is attributed to O-H-O scissoring bending. The bonds around 1300 cm^{-1} correspond to twisting vibrations and wagging motions [4]. Furthermore, it is assumed that the absorption band observed within the frequency range of $2126 - 1620$ cm^{-1} can be attributed to the stretching mode of gold hydrides (Au-H). The observation of gold-hydrogen complexes has been previously claimed based on infrared spectroscopy. Garcia et al. reported a weak band at 2126 cm^{-1} assigned to the Au-H stretching vibration, while Boccuzzi et al. identified a frequency at 1620 cm^{-1} as evidence for such a species. Both studies referenced the foundational work of Wang and Andrews, who generated gold hydride species via laser ablation and provided theoretical IR frequencies for validation [59, 60]. In our experiments, the presence of Au-H species confirmed by XRD analysis under different electric field, is likely to also be observed in FTIR spectra. Specifically, a broad band appears around 2000 cm^{-1} in the FTIR spectra, corresponding to these Au-H species. The depth of this band varies with applied electric field, being more pronounced under electric field of 10 and 15 V/cm. The peaks between 1500 to 1000 cm^{-1}, were allocated to the stretch modes of (CO_3) carbonate complexes connected to a metal. It can be presented in the form of (Au-OCO_2 or Au-OCO_2H), which indicates carbonate or bicarbonate. In fact, Au or AuH can connect to a carboxyl group. As observed in the XRD analysis, Au-H was detected at certain electric fields. Therefore, both carbonate and bicarbonate can be seen in FTIR analysis. The existence of carbonate complexes on the gold NPs probably confirmed the presence of CO_2 which is soluble in water or in the process of preparation for analysis, is exposed to air. Also, this chemical group (CO_3) may verify the existence of Au-O compounds on the surface of gold particles [61]. As shown in the figure, the peak indicates carbonate exists in all electric fields, but their intensity and forms are different. Additionally, in the electric fields of 10 and 15 V/cm, the vibrations associated with the CO_3 band are weaker than those observed in the other fields; in fact, fewer bands are associated with CO_3. We hypothesize that the interaction between hydrogen and gold under these

Table 1. Surface Plasmon resonance (SPR) as well as the main absorption peak for gold NPs at electric fields of: 0 V/cm, 5 V/cm, 10 V/cm, 15 V/cm, 20 V/cm, 25 V/cm.

Electric field (V/cm)	0	5	10	15	20	25
Absorbance	0.05	0.2	0.06	0.17	0.08	0.17
Wavelength (nm)	541.5	547	536	552.5	540	546

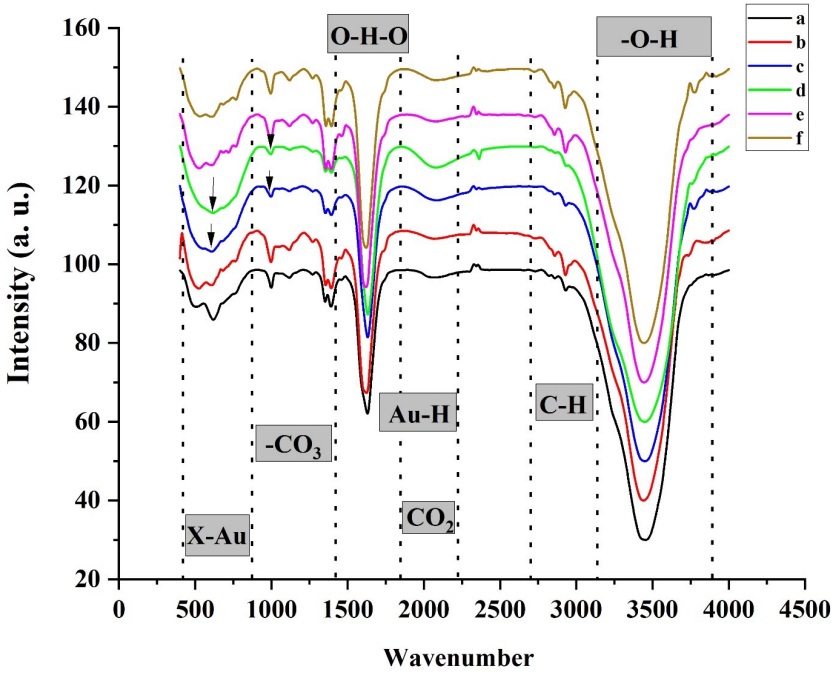

Figure 7. FT-IR spectra of colloidal Au NPs prepared by laser ablation in distilled water at electric fields of: (a) 0 V/cm, (b) 5 V/cm, (c) 10 V/cm, (d) 15 V/cm, (e) 20 V/cm, (f) 25 V/cm.

electric fields limits the number of gold atoms available for bonding with CO_3. It seems the number of available sites for carbonate adsorption appears to decrease due to the formation of Au-H bonds, which compete with other surface ligands; as a result, the intensity of carbonate-related peaks noticeably decreases in FTIR spectra under these electric fields [60]. The peaks observed between 800 and 400 cm^{-1} correspond to vibrations of gold (Au). We hypothesize that these vibrations are associated with Au-Au, Au-H, Au-C, and Au-O bonds. Typically, stretching vibrations related to metal-oxygen interactions occur in the range of 600 to 500 cm^{-1} [57]. This observation aligns with our the XRD results, which suggest the formation of gold oxide either within or on the surface of the gold NPs. Notably, in this region and under the electric field of 10 and 15 V/cm, the FTIR spectra exhibited broader peaks and altered overall shapes compared to other electric fields. It is assumed that the presence of non-spherical nanoparticles, as previously confirmed by TEM images, contributes to the broadening FTIR peaks in this region. Non- spherical nanoparticles often exhibit greater heterogeneity in size, shape and surface structure, which leads to variations in vibrational frequencies, resulting in peak broadening or, in some cases, the absence of distinct peaks [40, 62].

Furthermore, we assessed the zeta potential of the synthesized gold NPs using a nanosecond pulsed laser, as detailed in Table 2. The stability of the gold NPs against agglomeration is established through the correlation between the particle size distribution and their zeta potential. Coagulation is likely to occur when the zeta potential magnitude is low [10]. Colloidal stability is primarily associated with the presence of negative charges on the surfaces of particles. Numerous researchers have attributed the negative zeta potential observed in aqueous solutions to the presence of oxidized gold species, such as ($AuCO_3^{-1}$ and AuO^-) on the surfaces of the particles [63]. The creation of aggregates has been reported which emphasized the low value of negative charge around the particles in several experiments [64]. Two various hypotheses are surveyed to determine the source of the colloid stability: Either by a partial surface oxidation [65, 66] or by an excess of electrons produced during the plasma phase of the mechanism of the ablation process [67]. Moreover, the external electric field significantly impact the surface charge of nanoparticles. This highlights the crucial role of the electric field in modulating the electrostatic properties of laser-generated colloids, affecting not only particle nucleation and growth dynamics but also directly altering surface charge distribution [27–38]. In the analysis of the obtain data, it should first be noted that the formation of gold hydride is minimal, as evidenced by the weak intensity of the corresponding XRD peaks. This indicates that the presence of gold hydride in different electric fields has a negligible influence on the zeta potential. In fact, the observed zeta potential values are more likely attributed to the

Table 2. Zeta potential of gold nanoparticles produced at electric field of 0, 5, 10, 15, 20 and 25 V/cm.

Electric field (V/cm)	0	5	10	15	20	25
The value of zeta potential (mV)	−13.5	−6.74	−13.6	−15.1	−16.8	−2.14

tapped electrons within the plasma or the surface hydroxyl groups formed during the synthesis process [65–67]. In this experiment, a zeta potential value of −16.8 mV and a mobility of −1.317 (μm cm/Vs) were obtained at electric field strength of 20 V/cm, indicating the relative stability of the nanoparticles compared to other solutions. It seems that under this applied electric field a more efficient charge separation occurs within the plasma, resulting in a higher number of electrons being captured on the surface of the Au NPs. Also, it is assumed that the presence of Au_2O_3, suggests a partial oxidation of gold under this electric field. In Fact, increasing the electric field could enhance oxide formation probability by boosting plasma energy and acceleration electrons. As reported in previous studies, the presence of gold oxide can enhance the stability of nanoparticles. Consequently, this thin oxide layer, together with the increased surface charge, contributes to a higher zeta potential and enhanced colloidal stability. On the other hand, the lowest zeta potential value was observed under the applied electric field of 25 V/cm. This significant decrease in zeta potential could be attributed to the reduction of electrostatic repulsion and the increase tendency of gold NPs to adhere to each other, resulting in higher degrees of agglomeration. This observation is consistent with the TEM results, which revealed the presence of larger particles and clear signs of agglomeration. In fact, at this electric field, it assumed the induced dipole moment in the gold NPs, can drive them to align and form chain-like or aggregated. Consequently, the interfacial surface area decreased, leading to lower zeta potential value and indicating reduced colloidal stability [68].

4. Conclusion

In summary, we synthesized colloidal gold NPs without the use of chemical precursors by employing a nanosecond laser to irradiate a gold target in deionized water. We investigated the effects of an external electric field ($0-25$ V/cm) on the morphology and structure of the resulting products. The XRD revealed a pronounced effect of the applied electric field on hydrogen incorporation in the crystalline structure of Au nanoparticles. The formation of gold hydride exhibited a non-monotonic behavior with increasing electric field strength. In our experiment, the tendency of hydrogen to interact with gold was enhanced under specific electric fields, whereas it was suppressed under another field regime. Also, the presence of a peak around 2000 cm^{-1} in the FTIR spectrum further supported the likelihood of hydrogen – gold interactions under the applied experimental conditions. The TEM images of all samples exhibited predominantly spherical (or nearly spherical) particles, However, at an electric field strength of 15 V/cm, some Nano-rod-like structures were also observed. The presence of these non- spherical NPs at this field strength may contribute to the broadening of the FTIR peaks around 600 cm^{-1}. The slight blues shift observed in the UV-Vis spectrum could indicated the interaction between gold and hydrogen species. While the presence of non- spherical NPs caused a slight red shift in the UV-Vis spectrum. Additionally, the application of an external electric field of 20 V/cm conferred moderate colloidal stability to the synthesized NPs. This research serves as a foundation for further studies aimed at enhancing the effective incorporation of ions, such as hydrogen, into the structures of gold nanoparticles for functional applications, including optical hydrogen sensors.

Authors Contribution
Parisa Ojaroody was involved in all aspect of the manuscript preparation and performing experiments. Mohammadreza Hantehzadeh participated in the study design, performing experiment, involving data interpretation and reviewing the manuscript. Elham Darabi was involved in experimental data analyses, preparation of figures, and reviewing the manuscript.

Availability of data and materials
The statistical data supporting this study is presented in the results section. The raw data underlying these findings is available upon request from the corresponding author.

Conflict of interests
The authors declare that they have no known competing financial interests or personal relationships that could have appeared to influence the work reported in this paper.

References

[1] L. Gentile, H. Mateos, A. Mallardi, M. Dell'Aglio, A. De Giacomo, N. Cioffi, and G. Palazzo. Gold nanoparticles obtained by ns-pulsed laser ablation in liquids (ns-PLAL) are arranged in the form of fractal clusters. *Journal of Nanoparticle Research*, **23**(2):35, (2021). DOI: https://doi.org/10.1007/s11051-021-05140-5.

[2] M. Alheshibri, S. Akhtar, A. Al Baroot, K.A. Elsayed, H.S. Al Qahtani, and Q.A. Drmosh. Template-free single-step preparation of hollow CoO nanospheres using pulsed laser ablation in liquid enviroment. *Arabian Journal of Chemistry*, **14**(9):103317, (2021). DOI: https://doi.org/10.1016/j.arabjc.2021.103317.

[3] W. Qian, M. Murakami, Y. Ichikawa, and Y. Che. Highly efficient and controllable PEGylation of gold nanoparticles prepared by femtosecond laser ablation in water. *Journal of Physical Chemistry C*, **115**(47):23293–23298, (2011). DOI: https://doi.org/10.1021/jp2079567.

[4] A.A. Salim, S.K. Ghoshal, H. Bakhtiar, G. Krishnan, and H.H.J. Sapingi. Pulse laser ablated growth of Au-Ag nanocolloids: Basic insight on physiochemical attributes. *Journal of Physics: Conference Series*, **1484**:012011, (2020). DOI: https://doi.org/10.1088/1742-6596/1484/1/012011.

[5] S.A. Chinchulkar, P. Patra, D. Dehariya, T. Appidi, and A.K. Rengan. Gold nanoparticle–based biosensing applications and fundamentals of sensor technology: principles and novel designs. *Fundamentals of Sensor Technology*, pages 669–723, (2023). DOI: https://doi.org/10.1016/B978-0-323-88431-0.00014-4.

[6] Z. Hua, T. Yu, D. Liu, and Y. Xianyu. Recent advances in gold nanoparticles-based biosensors for food safety detection. *Biosensors and Bioelectronics*, **179**:113076, (2021). DOI: https://doi.org/10.1016/j.bios.2021.113076.

[7] H. Ito, T. Saito, T. Miyahara, C. Zhong, and M. Sawamura. Gold (I) hydride intermediate in catalysis: Dehydrogenative alcohol silylation catalyzed by gold (I) complex. *Organometallics*, **28**(16):4829–4840, (2009). DOI: https://doi.org/10.1021/om900445w.

[8] Y. Nishijima, T. Kurotsu, N. Yamasaku, H. Takahashii, K. Kurihara, T. Beni, S. Okazaki, T. Arakawa, A. Balčytis, G. Seniutinas, and S. Juodkazis. Improvement and stabilization of optical hydrogen

sensing ability of Au-Pd alloys. *Optics Express*, **28**(17):25383–25391, (2020).
DOI: https://doi.org/10.1364/OE.398784.

[9] A.K. Pathak, S. Verma, N. Sakda, C. Viphavakit, R. Chitaree, and B.A. Rahman. Recent advances in optical hydrogen sensor including use of metal and metal alloys: A review. *Photonics*, **10**(2):122, (2023).
DOI: https://doi.org/10.3390/photonics10020122.

[10] A. Lévy, M. de Anda Villa, G. Laurens, V. Blanchet, J. Bozek, J. Gaudin, L. Emily, M. Stephane, M. Pierre, R. Aleksandar, and D. Amans. Surface chemistry of gold nanoparticles produced by laser ablation in pure and saline water. *Langmuir*, **37**(19):5783–5794, (2021).
DOI: https://doi.org/10.1021/acs.langmuir.1c00092.

[11] N. Tarasenka, A. Butsen, V. Pankov, T. Velusamy, D. Mariotti, and N. Tarasenko. Laser assisted preparation of doped ZnO nanocrystals. *Nano-Structures & Nano-Objects*, **12**:210–219, (2017).
DOI: https://doi.org/10.1016/j.nanoso.2017.10.008.

[12] V. Amendola and M. Meneghetti. What controls the composition and the structure of nanomaterials generated by laser ablation in liquid solution? *Physical Chemistry Chemical Physics*, **15**(9):3027–3046, (2013).
DOI: https://doi.org/10.1039/C2CP42895D.

[13] T. Asahi, T. Sugiyama, and H. Masuhara. Laser fabrication and spectroscopy of organic nanoparticles. *Accounts of Chemical Research*, **41**(12):1790–1798, (2008).
DOI: https://doi.org/10.1021/ar800125s.

[14] A.A. Manda, K.A. Elsayed, U.I. Gaya, S.A. Haladu, I. Ercan, F. Ercan, and A.L. Al-Otaibi. Enhanced photocatalytic degradation of methylene blue by nanocomposites prepared by laser ablation of Bi on CNT-α-Fe_2O_3 nanoparticles. *Optics & Laser Technology*, **155**: 108430, (2022).
DOI: https://doi.org/10.1016/j.optlastec.2022.108430.

[15] V. Amendola and M. Meneghetti. Laser ablation synthesis in solution and size manipulation of noble metal nanoparticles. *Physical Chemistry Chemical Physics*, **11**(20):3805–3821, (2009).
DOI: https://doi.org/10.1039/B900654K.

[16] M. Bakhtiari and E. Hantehzadeh, M.a nd Darabi. The effect of applied electric field on the micromorphology of Pt nanoparticles synthesized by laser ablation. *Microscopy Research and Technique*, **84**(12):3171–3181, (2021).
DOI: https://doi.org/10.1002/jemt.23875.

[17] S. Barcikowski and G. Compagnini. Advanced nanoparticle generation and excitation by lasers in liquids. *Physical Chemistry Chemical Physics*, **15**(9):3022–3026, (2013).
DOI: https://doi.org/10.1039/C2CP90132C.

[18] A.A. Manda, Q.A. Drmosh, K.A. Elsayed, A.L. Al-Alotaibi, I.O. Alade, S.A. Onaizi, and A. Elhassan. Highly efficient UV–visible absorption of TiO_2/Y_2O_3 nanocomposite prepared by nanosecond pulsed laser ablation technique. *Arabian Journal of Chemistry*, **15** (8):104004, (2022).
DOI: https://doi.org/10.1016/j.arabjc.2022.104004.

[19] K.A. Elsayed, M. Alomari, Q.A. Drmosh, A.A. Manda, S.A. Haladu, and I.O. Alade. Anticancer activity of TiO_2/Au nanocomposite prepared by laser ablation technique on breast and cervical cancers. *Optics & Laser Technology*, **149**:107828, (2022).
DOI: https://doi.org/10.1016/j.optlastec.2021.107828.

[20] Q. Zhang, M. Honda, S.A. Kulinich, and Y. Ichikawa. Generation of nanomaterials in dopant-containing liquid via pulsed laser ablation. *Applied Surface Science*, **541**:148438, (2021).
DOI: https://doi.org/10.1016/j.apsusc.2020.148438.

[21] C.Y. Shih, R. Streubel, J. Heberle, A. Letzel, M.V. Shugaev, C. Wu, and L.V. Zhigilei. Two mechanisms of nanoparticle generation in picosecond laser ablation in liquids: the origin of the bimodal size distribution. *Nanoscale*, **10**(15):6900–6910, (2018).
DOI: https://doi.org/10.1039/C7NR08614H.

[22] A. Kanitz, M.R. Kalus, E.L. Gurevich, A. Ostendorf, S. Barcikowski, and D. Amans. Review on experimental and theoretical investigations of the early stage, femtoseconds to microseconds processes during laser ablation in liquid-phase for the synthesis of colloidal nanoparticles. *Plasma Sources Science and Technology*, **28**(10): 103001, (2019).
DOI: https://doi.org/10.1088/1361-6595/ab3dbe.

[23] S. Reich, A. Letzel, A. Menzel, N. Kretzschmar, B. Gökce, S. Barcikowski, and A. Plech. Early appearance of crystalline nanoparticles in pulsed laser ablation in liquids dynamics. *Nanoscale*, **11**(14):6962–6969, (2019).
DOI: https://doi.org/10.1039/C9NR01203F.

[24] R. Streubel, G. Bendt, and B. Gökce. Pilot-scale synthesis of metal nanoparticles by high-speed pulsed laser ablation in liquids. *Nanotechnology*, **27**(20):205602, (2016).
DOI: https://doi.org/10.1088/0957-4484/27/20/205602.

[25] R. Streubel, S. Barcikowski, and B. Gökce. Continuous multigram nanoparticle synthesis by high-power, high-repetition-rate ultrafast laser ablation in liquids. *Optics Letters*, **41**(7):1486–1489, (2016).
DOI: https://doi.org/10.1364/OL.41.001486.

[26] Q.A. Drmosh, I.O. Alade, K. Alkanad, G. Alnaggar, A. Khan, M.Y. Khan, and S.A. Onaizi. Fabrication of Z-scheme TiO_2/BP/g-C_3N_4 nanocomposite via pulsed laser ablation in liquid for photocatalytic overall water splitting. *Optical Materials*, **128**:112428, (2022).
DOI: https://doi.org/10.1016/j.optmat.2022.112428Get rights and content.

[27] M. Cutroneo, V. Havranek, J. Vacik, L. Torrisi, L. Silipigni, P. Malinsky, and A. Mackova. Gold nanoparticles produced by laser ablation in distilled water assisted by electric field. . *Radiation Effects and Defects in Solids*, **177**(11-12):1232–1242, (2022).
DOI: https://doi.org/10.1080/10420150.2022.2163719.

[28] D. Sapkota, Y. Li, O.R. Musaev, J.M. Wrobel, and M.B. Kruger. Effect of electric fields on tin nanoparticles prepared by laser ablation in water. *Journal of Laser Applications*, **29**(1), (2017).
DOI: https://doi.org/10.2351/1.4963270.

[29] H. Mozaffari and M.H. Mahdieh. Enhancement of ablation rate and production of colloidal nanoparticles by irradiation of metals with nanosecond pulsed laser in presence of external electric field. *Physics Letters A*, **383**(7):646–654, (2019).
DOI: https://doi.org/10.1016/j.physleta.2019.01.005.

[30] S. Moniri, M.R. Hantehzadeh, M. Ghoranneviss, and M. Asadabad. Study of the optical and structural properties of Pt nanoparticles prepared by laser ablation as a function of the applied electric field. *Applied Physics A*, **123**(11):684, (2017).
DOI: https://doi.org/10.1007/s00339-017-1311-9.

[31] J. Xiao, P. Liu, C.X. Wang, and G.W. Yang. External field-assisted laser ablation in liquid: An efficient strategy for nanocrystal synthesis and nanostructure assembly. *Progress in Materials Science*, **87**:140–220, (2017).
DOI: https://doi.org/10.1016/j.pmatsci.2017.02.004.

[32] H. Mozaffari and M.H. Mahdieh. Synthesis of colloidal aluminum nanoparticles by nanosecond pulsed laser and the effect of external electric field and laser fluence on ablation rate. *Optics & Laser Technology*, **126**:106083, (2020).
DOI: https://doi.org/10.1016/j.optlastec.2020.106083.

[33] X.Z. Lin, P. Liu, J.M. Yu, and G.W. Yang. Synthesis of CuO nanocrystals and sequential assembly of nanostructures with shape-dependent optical absorption upon laser ablation in liquid. *Journal of Physical Chemistry C*, **113**(40):17543–17547, (2009).
DOI: https://doi.org/10.1021/jp907237q.

[34] M. Razaghianpour, M.R. Hantehzadeh, A.H. Sari, and E. Darabi. Electric field assisted-laser ablation of cu nanoparticles in ethanol and investigation of their properties. *Optical and Quantum Electronics*, **54**(1):23, (2022).
DOI: https://doi.org/10.1007/s11082-021-03286-z.

[35] R. Gagrani, N. Patra, P. Rajagopalan, V. Singh, and I.A. Palani. Influence of laser parameters in generating the NiTi nanoparticles with a rotating target using underwater solid state Nd:YAG laser ablation. *IOP Conference Series: Materials Science and Engineering*, **149**:012034, (2016).
DOI: https://doi.org/10.1088/1757-899X/149/1/012034.

[36] A. Momeni and M.H. Mahdieh. Double-pulse nanosecond laser ablation of silicon in water. *Laser Physics Letters*, **12**(7):076102, (2015).
DOI: https://doi.org/10.1088/1612-2011/12/7/076102.

[37] S. Kohsakowski, A. Santagata, M. Dell'Aglio, A. de Giacomo, S. Barcikowski, P. Wagener, and B. Gökce. High productive and continuous nanoparticle fabrication by laser ablation of a wire-target in a liquid jet. *Applied Surface Science*, **403**:487–499, (2017).
DOI: https://doi.org/10.1016/j.apsusc.2017.01.077.

[38] M.H. Mahdieh and A. Khosravi. Colloidal brass nanoparticles produced by pulsed laser ablation in deionized water and the effect of external electric field on particle size characteristics and ablation rate. *Nano-Structures & Nano-Objects*, **24**:100580, (2020).
DOI: https://doi.org/10.1016/j.nanoso.2020.100580.

[39] D. Salley, G. Keenan, J. Grizou, A. Sharma, S. Martín, and L. Cronin. A nanomaterials discovery robot for the Darwinian evolution of shape programmable gold nanoparticles. *Nature Communications*, **11**(1):2771, (2020).
DOI: https://doi.org/10.1038/s41467-020-16501-4.

[40] U. Ulusoy. A review of particle shape effects on material properties for various engineering applications: from macro to nanoscale. *Minerals*, **13**(1):91, (2023).
DOI: https://doi.org/10.3390/min13010091.

[41] V.F. Degtyareva. Crystal structure of gold hydride. *Journal of Alloys and Compounds*, **645**:S128–S131, (2015).
DOI: https://doi.org/10.1016/j.jallcom.2014.12.262.

[42] K.B. Beć and C.W. Huck. Breakthrough potential in near-infrared spectroscopy: Spectra simulation. A review of recent developments. *Frontiers in Chemistry*, **7**:48, (2019).
DOI: https://doi.org/10.3389/fchem.2019.00048.

[43] L. Rolinger, M. Rüdt, and J. Hubbuch. A critical review of recent trends, and a future perspective of optical spectroscopy as PAT in biopharmaceutical downstream processing. *Analytical and Bioanalytical Chemistry*, **412**(9):2047–2064, (2020).
DOI: https://doi.org/10.1007/s00216-020-02407-z.

[44] M. Alhujaily, M.S. Jabir, U.M. Nayef, T.M. Rashid, G.M. Sulaiman, K.A. Khalil, and S.F. Jawad. Au/ZnO nanocomposites prepared by laser ablation for enhancement of antibacterial activity and cytotoxic properties against cancer cells. *Metals*, **13**(4):735, (2023).
DOI: https://doi.org/10.3390/met13040735.

[45] E. Solati and D. Dorranian. Comparison between silver and gold nanoparticles prepared by pulsed laser ablation in distilled water. *Journal of Cluster Science*, **26**(3):727–742, (2015).
DOI: https://doi.org/10.1007/s10876-014-0732-2.

[46] Y. Hu, H. Zhang, P. Wu, H. Zhang, B. Zhou, and C. Cai. Bimetallic Pt–Au nanocatalysts electrochemically deposited on graphene and their electrocatalytic characteristics towards oxygen reduction and methanol oxidation. *Physical Chemistry Chemical Physics*, **13**(9): 4083–4094, (2011).
DOI: https://doi.org/10.1039/C0CP01998D.

[47] L. Zhao, N. Heinig, and K.T. Leung. Formation of au–pt alloy nanoparticles on a si substrate by simple dip-coating at room temperature. *Langmuir*, **29**(3):927–931, (2013).
DOI: https://doi.org/10.1021/la303809m.

[48] S.Y. Sarvadiy, A.K. Gatin, M.V. Grishin, V.A. Kharitonov, N.N. Kolchenko, N.V. Dokhlikova, and B.R. Shub. Electric field–prevented adsorption of hydrogen on supported gold nanoparticles. *Gold Bulletin*, **52**(2):61–67, (2019).
DOI: https://doi.org/10.1007/s13404-019-00253-1.

[49] M.V. Grishin, A.K. Gatin, E.K. Golubev, N.V. Dokhlikova, S.A. Ozerin, S.Y. Sarvadii, and B.R. Shub. Interaction of gold and nickel nanoparticles with molecular hydrogen and carbon monoxide in the presence of an electric field. *Colloid Journal*, **85**(1):16–24, (2023).
DOI: https://doi.org/10.1134/S1061933X22600464.

[50] J.M. Koehler, N. Visaveliya, and A. Knauer. Controlling formation and assembling of nanoparticles by control of electrical charging, polarization, and electrochemical potential. *Nanotechnology Reviews*, **3**(6):553–568, (2014).
DOI: https://doi.org/10.1515/ntrev-2014-0006.

[51] P. Liu, H. Cui, C.X. Wang, and G.W. Yang. From nanocrystal synthesis to functional nanostructure fabrication: laser ablation in liquid. *Physical Chemistry Chemical Physics*, **12**(16):3942–3952, (2010).
DOI: https://doi.org/10.1039/B918759F.

[52] J. Fontana, G.K. da Costa, J.M. Pereira, J. Naciri, B.R. Ratna, P. Palffy-Muhoray, and I. Carvalho. Electric field induced orientational order of gold nanorods in dilute organic suspensions. *Applied Physics Letters*, **108**(8), (2016).
DOI: https://doi.org/10.1063/1.4942969.

[53] D. Li, T. Wang, S. Chen, Q. Liu, Y. Xie, and C. Liu. Experimental investigation on droplet deformation and breakup under uniform DC electric field. *Microgravity Science and Technology*, **32**(5):837–845, (2020).
DOI: https://doi.org/10.1007/s12217-020-09808-w.

[54] D. Sil, E. Lane, C.a nd Glor, K.D. Gilroy, S. Sylla, B. Barbiellini, and E. Borguet. Synthesis and Properties of Au Hydride. *ChemistrySelect*, **14**(14):4287–4292, (2019).
DOI: https://doi.org/10.1002/slct.201900925.

[55] A.K. Sahu and S. Raj. Understanding the coupling mechanism of gold nanostructures by finite-difference time-domain method. *International Journal of Nanoscience*, **21**:2250007, (2022).
DOI: https://doi.org/10.1142/S0219581X22500077.

[56] S.T. Van Der Post, C.S. Hsieh, M. Okuno, Y. Nagata, H.J. Bakker, M. Bonn, and J. Hunger. Strong frequency dependence of vibrational relaxation in bulk and surface water reveals sub-picosecond structural heterogeneity. *Nature Communications*, **6**(1):8384, (2015).
DOI: https://doi.org/10.1038/ncomms9384.

[57] S. Adib Amini, A.H. Sari, and D. Dorranian. Optical properties of synthesized Au/Ag Nanoparticles using 532 nm and 1064 nm pulsed laser ablation: effect of solution concentration. *SN Applied Sciences*, **5**(4):122, (2023).
DOI: https://doi.org/10.1007/s42452-023-05310-1.

[58] N.Z.A. Naharuddin, A.R. Sadrolhosseini, M.H. Abu Bakar, N. Tamchek, and M.A. Mahdi. Laser ablation synthesis of gold nanoparticles in tetrahydrofuran. *Optical Materials Express*, **10**(2):323–331, (2020).
DOI: https://doi.org/10.1364/OME.381427.

[59] A. Manzoli, M.a nd Chiorino, F. Vindigni, and F. Boccuzzi. Hydrogen interaction with gold nanoparticles and clusters supported on different oxides: A FTIR study. *Catalysis Today*, **181**(1):62–67, (2012).
DOI: https://doi.org/10.1016/j.cattod.2011.07.029.

[60] I.P. Silverwood, S.M. Rogers, S.K. Callear, S.F. Parker, and C.R.A. Catlow. Evidence for a surface gold hydride on a nanostructured gold catalyst. *Chemical Communications*, **52**(3):533–536, (2016).
DOI: https://doi.org/10.1039/C5CC06118K.

[61] J.P. Sylvestre, S. Poulin, A.V. Kabashin, E. Sacher, M. Meunier, and J.H. Luong. Surface chemistry of gold nanoparticles produced by laser ablation in aqueous media. *Journal of Physical Chemistry B*, **108**(43):16864–16869, (2004).
DOI: https://doi.org/10.1021/jp047134.

[62] O. Diwald and T. Berger. Metal Oxide Nanoparticles, 2 Volume Set: Formation, Functional Properties, and Interfaces. John Wiley & Sons (3):533–536, (2021).
DOI: https://doi.org/10.1002/9781119436782.

[63] H. Mateos, R.A. Picca, A. Mallardi, M. Dell'Aglio, A. De Giacomo, N. Cioffi, and G. Palazzo. Effect of the surface chemical composition and of added metal cation concentration on the stability of metal nanoparticles synthesized by pulsed laser ablation in water. *Applied Sciences*, **10**(12):4169, (2020).
DOI: https://doi.org/10.3390/app10124169.

[64] S. Reich, P. Schönfeld, P. Wagener, A. Letzel, S. Ibrahimkutty, B. Gökce, and A. Plech. Pulsed laser ablation in liquids: Impact of the bubble dynamics on particle formation. *Journal of Colloid and Interface Science*, **489**:106–113, (2017).
DOI: https://doi.org/10.1016/j.jcis.2016.08.030.

[65] H. Muto, K. Yamada, K. Miyajima, and F. Mafuné. Estimation of surface oxide on surfactant-free gold nanoparticles laser-ablated in water. *Journal of Physical Chemistry C*, **111**(46):17221–17226, (2007).
DOI: https://doi.org/10.1021/jp075582m.

[66] M. Vivian, R. Christoph, B. Felix, H. Ulrich, N. Hermann, and B. Stephan. Situ Non-DLVO Stabilization of Surfactant-Free, Plasmonic Gold Nanoparticles: Effect of Hofmeister's Anions. page 47048, (2014).
DOI: https://doi.org/10.1021/la404556a.

[67] M. Dell'Aglio, V. Motto-Ros, F. Pelascini, I.B. Gornushkin, and A. De Giacomo. Investigation on the material in the plasma phase by high temporally and spectrally resolved emission imaging during pulsed laser ablation in liquid (PLAL) for NPs production and consequent considerations on NPs formation. *Plasma Sources Science and Technology*, **28**(8):085017, (2019).
DOI: https://doi.org/10.1088/1361-6595/ab369b.

[68] F.A. Deader, Y. Abbas, A. Qurashi, M. Al-Qutayri, V. Chan, and M.D. Rezeq. Electric field-driven self-assembly of gold nanoparticle monolayers on silicon substrates. *Langmuir*, **39**(44):15766–15772, (2023).
DOI: https://doi.org/10.1021/acs.langmuir.3c02351L.